

# Comparative Study between EKF, SVSF, Combined SVSF-EKF, and ASVSF Approaches based Scale Estimation of Monocular SLAM

Elhaouari Kobzili<sup>1</sup> <sup>a</sup>, Ahmed Allam<sup>2</sup> and Cherif Larbes<sup>1</sup>

<sup>1</sup>Electronic Department, National Polytechnic School, 10 Avenue des Frères Oudek, ElHarrach, BP 182, Algiers, Algeria

<sup>2</sup>Automatic Department, National Polytechnic School, 10 Avenue des Frères Oudek, ElHarrach, BP 182, Algiers, Algeria

**Keywords:** Monocular SLAM, Scale Estimation, Robust Filter, Multi-rate.

**Abstract:** This paper presents a comparative study of scale recovering in monocular simultaneous localization and mapping (Mono-SLAM) by adopting and adapting four estimators into a multi-rate fusion mechanism and considering the scale as an element of the state vector. These estimators are: extended Kalman filter (EKF), smooth variable structure filter (SVSF), combined SVSF-EKF, and particularly adaptive smooth variable structure filter (ASVSF). The use of the ASVSF estimator represents the novelty of this paper because it provides a robust estimation of the trajectory scale as well as the covariance matrix at each iteration. This later represents the estimation incertitude. A second sensor is involved (inertial measurement unit (IMU)) as a reference to align the up to scale trajectory provided by the Mono-SLAM box. The designed system allows finding the scale factor with a rate not further than the IMU frequency and avoids complex synchronization. In order to outline the limitation of each estimator used for scale recovering, a deep analysis of the proposed approaches in terms of robustness, stability, accuracy, and real-time constraint was carried out.

## 1 INTRODUCTION

The autonomous navigation task of an unmanned aerial vehicle (UAV) is an active field. However the localization of UAV in the environment of navigation is crucial to realize its missions. To safely navigate the robot, it must perceive and recognize its environment. To deal with these requirements, the UAV must be equipped with the simultaneous localization and mapping (SLAM) module. Recently, the world has seen a sophisticated SLAM, based just on a monocular camera (Mono-SLAM). The Mono-SLAM problems are not completely solved, they are still under improvement. The challenge of Mono-SLAM approaches is to develop a solution of localization and mapping using just one camera with a compromise between price and algorithmic complexity. In this context many frameworks have been proposed in order to provide a good estimated pose as parallel tracking and mapping (PTAM) (Klein and Murray, 2007) large scale direct monocular simultaneous localization and mapping (LSD-SLAM) (Engel and Cremers, 2014), a versatile and accurate Monocular SLAM System (ORB-SLAM) (Mur-Artal et al., 2015), and Continuous Lo-

calization and Mapping in a Dynamic World (CD-SLAM) (Pirker et al., 2011). With respect to the state-of-the-art, all the previous Mono-SLAMs provide a pose up to scale and suffer from the scale ambiguity. In fact, this Mono-SLAM problem is due to the physical limitation of depth measurement. The scale error drifts by time, so it needs to be recovered at each step. Recovering the scale means that a robot has instantly a metric pose and a realistic interpretation of the evolution area. Many approaches and methods have been proposed to solve the scale problem. However, many authors have tackled the scale problem by designing sophisticated algorithms, based on the same frames which are exploited by the Mono-SLAM box. Other researchers recommended to consider the Mono-SLAM as a box which provides a pose up to scale, and involves other sensors as references. This type of solution can be more suited to scale recovery. These sensors can ensure a continuous localization separately from the Mono-SLAM box. With a sensor of high rate, it is possible to find the scale factor long times before processing a new pose (up to scale) provided by the Mono-SLAM box.

This paper is based on Gabriel Nutzi (Nutzi et al., 2011) efforts, the inertial measurement unit (IMU) data is considered as a reference to recover the ab-

<sup>a</sup>  <https://orcid.org/0000-0002-3112-9347>

solute scale. We elaborate a multi-rate fusion mechanism which functions on irregular integration time. To get a dynamic estimation of the scale, it is considered as an element of the state vector. Fortunately, this situation is possible by enforcing the pose provided by the two boxes (Mono-SLAM and IMU) to be in the same scale. This paper is an extension of our works originally presented in (Kobzili et al., 2017a) and (Kobzili et al., 2017b). The major difference is to involve the ASVSF as an estimator to find the metric trajectory.

The main contributions of this paper per rapport our previous works are:

- To involve exclusively, the ASVSF estimator to determine the scale factor.
- To investigate the scale estimation using robust filters, and developing those presented in (Kobzili et al., 2017a; Kobzili et al., 2017b).
- To compare and analyze the performances of scale estimation using EKF, SVSF, Combined SVSF-EKF, and ASVSF.
- To perform the comparative study of the estimators based scale recovering on real data.

This paper is organized as follows: Section. 2 gives the state-of-the-art of the different approaches developed for scale recovering. Section. 3 sketches the designed methodology of scale estimation and details the theories of the four estimators involving in the scale estimation process. Section. 4 deals with the presentation of the different results, by focusing on performance analysis of the proposed estimators. Section. 5 presents experiment results applied on a well known dataset. In this part, the four estimators are evaluated in terms of accuracy and real time constraint. Conclusion and further works are drawn in Section. 6.

## 2 RELATED WORK

### 2.1 Global Context

In the last decade, the SLAM task has been treated as an important field of research. However, it has been tackled primary as a filtering problem. The most popular solutions have been based on EKF-SLAM (Smith et al., 1990), Fast-SLAM (Montemerlo, 2003), and SLAM based state dependent Ricatti equation (SDRE) (Nemra, 2011). Recently, the SLAM has been solved by including vision sensors as the main sources of information in order to deal with many real life applications. In previous SLAM works, the scale

factor problem has not attracted so much attention (the SLAM resolved based on stereo-vision), because it is difficult to get depths of features easily (based on triangulation). Later, monocular SLAM became more and more a popular research topic (Klein and Murray, 2007; Engel and Cremers, 2014; Mur-Artal et al., 2015; Pirker et al., 2011; Davison et al., 2007; Civera et al., 2008; Eade and Drummond, 2006), by emerging complex imaging algorithms.

### 2.2 Scale Recovering based on Vision

Some authors proposed to exploit camera frames by extracting the adequate information needed for scale calculation. These approaches took advantage of the geometric nature of the environment by acquiring a known objects from the real world to update the scale value. We mention Davison et al (Davison et al., 2007) method, which is based on a referenced points existing in the navigating scene. In the same context, there are other authors who suggested to use the road map of the explored environment, by calculating the correspondent homography to decrease scale ambiguity (Simond and Rives, 2004; Dumortier et al., 2006; Scaramuzza and Siegwart, 2008; Kitt et al., 2007). In these previous solutions, the road was supposed flat, in order to keep the same distance between camera and road. To reach the scale performances of stereo-vision SLAMs, Shiyu Song (Song and Chandraker, 2014) includes a new cue combination framework for ground plane estimation. The same steps were followed by Johannes Grater (Grater et al., 2015). His work was articulated on the vanishing points. Another methodology of scale recovering based on extraction of object classes from images of the explored region (Botterill et al., 2013; Frost et al., 2016; Pillai and Leonard, 2015). These objects are compared with the real object's dimensions to reduce the scale drift. Unfortunately, the majority of previous approaches suffer from the level of images qualities, because they are influenced by severe environment changes. The utilization of a monocular camera only, can affect the reliability of the designed system, so it is very important to involve other types of sensors to find the absolute scale.

### 2.3 Particular Techniques of Scale Recovering

In a particular application of scale recovering, it is possible to profit from the non holonomic constraints of cars during turns (Scaramuzza et al., 2009). This approach has a restriction of regular turns in order to deal with the real scale. A specific scheme of scale

estimation was proposed in (Gutierrez-Gomez et al., 2012), in which the author based on performing a spectral analysis of vertical movement result of human walking by using empirical equations of human motion. To avoid scale ambiguity, some authors supposed to have partial information about the three dimensions of the environment geometry (Lothe, 2010).

## 2.4 Scale Recovering with an Additional Sensor

Another framework is to use other sensor with Mono-SLAM as adding another camera (Nister et al., 2006; Lemaire et al., 2007), in which the 3D coordinates of points are found based on the triangulation method, but this solution is very heavy in terms of computation. All Mono-SLAMs need to close the loop in order to eliminate drifts after realizing a considerable trajectory, in this context, a sophisticated solution of scale drift reducing is loop closing many times based on collaborative SLAM (Forste et al., 2013). The absolute position provided by the GPS is a good solution to recover the metric pose of the Mono-SLAM box (Agrawal and Konolige, 2006; Ikeda et al., 2007). Unfortunately, the GPS is not present all the time. In the same context, it is possible to involve many sensors into a mechanism scheme to limit the scale drift as in (Zachariah and Jansson, 2011). In this work, the author focused on airspeed and IMU sensors. The previous work encourages us to profit from the multi rate scheme due to the high frequency of scale recovery. Lv Qiang et al utilized Laser range in an indoor situation to find the scale of ORB-SLAM by filtering (Qiang et al., 2016). In this paper, the IMU is used to recover the scale based on a fusion mechanism. Recent efforts are given in (Strelow and Singh, 2004; Hol et al., 2007; Weiss and Siegart, 2011). They used very accurate inertial navigation system (INS) with high rate, but this solution can't deal with our future works (realizing a low cost solution for scale recovery). Our work, is based essentially on Gabriel Nutzi's work (Nutzi et al., 2011), in which the author designed two solutions: the first one is about the spline fitting task inspired and modified from the paper of Jung and Taylor (Jung and Taylor, 2001). The designed system didn't deal with the real time constraint. In the second solution, the author suggests to consider the scale factor as an element of the state vector. In the last work, the author utilizes a recent Mono-SLAM named PTAM (Klein and Murray, 2007), this last was restricted to indoor application. The author Gabriel Nutzi based his work on EKF, which gives a good result in ordinary conditions. These performances degraded in an outdoor

situation, especially in severe environmental changes, and automatically influenced the scale value quality.

## 2.5 Scale Recovering and the Robustness Involving

The method of scale factor recovery must provide the scale value with a high robustness, but unfortunately it is not the case for the EKF. To increase the robustness of scale estimation, we based our work on a new robust filter named smooth variable structure filter (SVSF) (Habibi, 2007). This filter is used into a multi-rate mechanism by considering the Mono-SLAM, and IMU data as measurements of the fusion process. To improve the robustness of scale estimation, a new solution is investigated, in which the smooth variable structure filter (SVSF) (Habibi, 2007) is combined with the EKF (Combined SVSF-EKF) (Habibi, 2008). This combination permits to stay near performance of EKF. This solution allows to benefit from the advantage of SVSF and EKF. The synergy created by the combination of the two filters permit to exercise the SVSF force outside the smoothing boundary layer, and to profit from the accuracy of EKF inside this layer. To go further in the comparison of the approaches proposed, it is suggested to investigate the improved version of SVSF named as adaptive smooth variable structure filter (ASVSF) (Gadsden and Habibi, 2010; Gadsden et al., 2011), in which, it is based on an adaptive boundary layer. All estimators suggested for scale estimation functioned into a multi-rate mechanism (Armesto et al., 2004). This paper is an extension of our previous works (Kobzili et al., 2017a; Kobzili et al., 2017b). However, a deep comparison between the scale approaches followed by a performance analysis are detailed in our paper sections.

## 3 METHODOLOGY

### 3.1 An Overview of the Designed System

#### 3.1.1 Parameters of the Designed System

We design a system able to provide a metric pose using Mono-SLAM data. This modular conception allows us to change the Mono-SLAM box easily without affecting the integrity of our system. All Mono-SLAMs provide a pose up to scale. The camera pose is defined in six dimensions (6D), three for Cartesian position  $X_{SLAM,k} = [x \ y \ z]^T$ , and three for angu-

lar position  $\phi_{SLAM,k} = [\varphi \ \theta \ \psi]^T$ . The camera's pose provides information about the trajectory, but it is not a metric position due to depth ambiguity. The rate of the Mono-SLAM suggested to be equal 20 Hz. In our simulation, the camera and the IMU are assumed to have the same gravity center. The IMU sensor provides accelerations, and angular rates with a frequency of 200 Hz, defined in the body frame  $a_{IMU}^b = [ax \ ay \ az]^T$ ,  $\omega_{IMU}^b = [p \ q \ r]^T$ .

To be near the reality, the output of Mono-SLAM is assumed to be affected by a zero mean Gaussian noise of standard deviation  $\sigma_v = 0.01m$ .

The standard deviation of noise affected accelerations measurements of IMU is given by  $\sigma_a = 2 \cdot 10^{-3}m/s^2$ , with a bias of  $\sigma_b = 3 \cdot 10^{-3}m/s^2$ . The gyros of the considered IMU affected by noise with a standard deviation value  $\sigma_g = 1.6968 \cdot 10^{-4}rad/s$ , and a bias  $\sigma_{bg} = 1.9393 \cdot 10^{-5}rad/s$ .

### 3.1.2 Synoptic Representation of the Designed System

The system consists of two fusion processes with the same prediction model based on a temporal motion. The updating is realized by considering two measurements coming from the Mono-SLAM and the IMU. The transfer of state variation is alternated between the two fusion processes into a multi rate mechanism. For more details about the designed system see Fig. 1,  $\hat{Y}_{v/i,k}$ : represents the state vector of our system. The notice  $v/i$  denotes vision and IMU. The matrix  $P_k$  is the covariance matrix, which is initialized by  $P_0$ .

## 3.2 Extended Kalman Filter Approach

The nonlinear prediction model proposed is given by: (1). This model is detailed by the full expression given by: (2). The scale factor is considered as an element of the state vector which is injected in the equations of position. For each step we get a new estimated scale based on the last measurement which is used to correct the Mono-SLAM poses.

$$\hat{Y}_{v/i,k} = f(x_{k-1}, v_{k-1}, a_{k-1}, \phi_{k-1}, \dot{\phi}_{k-1}, \lambda_{k-1}) + q_k \quad (1)$$

$$\hat{Y}_k = \begin{bmatrix} I_3 & \frac{TI_3}{\lambda_{k-1}} & \frac{T^2I_3}{2\lambda_{k-1}} & 0_3 & 0_3 & 0_{31} \\ 0_3 & I_3 & TI_3 & 0_3 & 0_3 & 0_{31} \\ 0_3 & 0_3 & I_3 & 0_3 & 0_3 & 0_{31} \\ 0_3 & 0_3 & 0_3 & I_3 & TI_3 & 0_{31} \\ 0_3 & 0_3 & 0_3 & 0_3 & I_3 & 0_{31} \\ 0_{13} & 0_{13} & 0_{13} & 0_{13} & 0_{13} & 1 \end{bmatrix} \hat{Y}_{k-1} \quad (2)$$

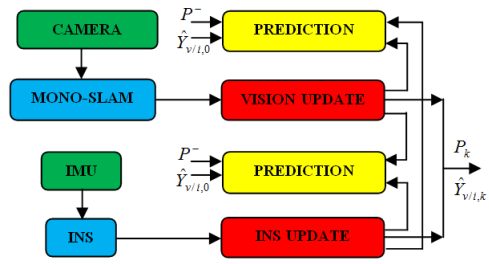


Figure 1: An overview of the designed system.

The state vector elements are defined in the navigation frame, where  $x_k \in R^{3 \times 1}$  is the position vector without scale,  $v_k \in R^{3 \times 1}$  and  $a_k \in R^{3 \times 1}$  represent the velocity and acceleration vectors of the Camera-IMU system. The Euler angles are  $\phi_k \in R^{3 \times 1}$ , the vector  $\dot{\phi}_k \in R^{3 \times 1}$  is Euler angles velocities. The parameter  $\lambda_k$  is the scale factor. The vector  $q_k$  is a Gaussian noise that affected our system. The index  $v/i$  defines the prediction and the measurement in the case of vision or IMU. Where  $I_3, 0_3$  mean an identity and zero matrixes of dimension  $3 \times 3$ , and  $0_{31}, 0_{13}$  mean successfully column and raw vectors of elements equal to zero.

Our prediction model is a nonlinear system. Its Jacobian matrix ( $F$ ) is given by: (3).

$$\begin{bmatrix} I_3 & \frac{TI_3}{\lambda_{k-1}} & \frac{T^2I_3}{2\lambda_{k-1}} & 0_3 & 0_3 & -\frac{Tv_{k-1}}{\lambda_{k-1}^2} - \frac{T^2a_{k-1}}{2\lambda_{k-1}^2} \\ 0_3 & I_3 & TI_3 & 0_3 & 0_3 & 0_{31} \\ 0_3 & 0_3 & I_3 & 0_3 & 0_3 & 0_{31} \\ 0_3 & 0_3 & 0_3 & I_3 & TI_3 & 0_{31} \\ 0_3 & 0_3 & 0_3 & 0_3 & I_3 & 0_{31} \\ 0_{13} & 0_{13} & 0_{13} & 0_{13} & 0_{13} & 1 \end{bmatrix} \quad (3)$$

Its prior covariance matrix is given by: (4)

$$P^- = FP_kF^T + Q \quad (4)$$

$P^-$ : represents the prior covariance matrix, and  $Q$  is the noise covariance matrix. The matrix  $P_k$  defines the posterior covariance matrix which is initialized by  $P_0$ . To involve the multi-rate mechanism, it is suggested to consider that there are two measurement sources (Camera and IMU). When the Mono-SLAM box provides a new measurement, our system calculates a prediction of the state vector using the last values and doing the updating by taking into consideration the Mono-SLAM data. To deal with the appropriate time of prediction, we use the equation (5) to calculate the time of integration.

$$T = t - T_a \quad (5)$$

$t$ : is the time of calculation defined by the loop of execution (internal clock). The variable  $T_a$  represents

the time of the last estimated vector. In case of IMU data, the estimation process has to recover the scale many times due to its high frequency compared to the Mono-SLAM observation.

The two measurement models used in our paper for the Mono-SLAM and IMU boxes are given by equations (6) and (9) which are cited afterwards. The state vector observation of our system is goes through two differents observation matrices depends on measurements provided by the sensor used.

$$Y_{vm,k} = H_v Z_{SLAM,k} \quad (6)$$

The observation matrix of Mono-SLAM measurements is given by (7).

$$H_v = \begin{bmatrix} I_3 & 0_3 & 0_3 & 0_3 & 0_3 & 0_{3 \times 1} \\ 0_3 & 0_3 & 0_3 & I_3 & 0_3 & 0_{3 \times 1} \end{bmatrix} \quad (7)$$

The measurement vector provided by the Mono-SLAM box is defined by: (8).

$$Z_{SLAM,k} = [X_{SLAM,k} \quad 0_{1 \times 6} \quad \phi_{SLAM,k} \quad 0_{1 \times 3} \quad 0]^T \quad (8)$$

$$Y_{im,k} = H_i Z_{IMU,k} \quad (9)$$

The observation matrix of IMU measurements is given as follows by: (10).

$$H_i = \begin{bmatrix} 0_3 & 0_3 & I_3 & 0_3 & 0_3 & 0_{3 \times 1} \\ 0_3 & 0_3 & 0_3 & 0_3 & I_3 & 0_{3 \times 1} \end{bmatrix} \quad (10)$$

The measurement vector provided by the IMU box is defined by: (11).

$$Z_{IMU,k} = [0_{1 \times 6} \quad a_{IMU,k} \quad 0_{1 \times 3} \quad \dot{\phi}_{IMU,k} \quad 0]^T \quad (11)$$

The acceleration vector was calculated in the navigation frame using IMU data which is given by: (12).

$$a_{IMU,k} = C_b^n(k-1) a_{IMU}^b + g^n \quad (12)$$

The Euler angles velocities are defined in the navigation frame by the following equation (13).

$$\dot{\phi}_{IMU,k} = E_b^n(k-1) \omega^b(k) \quad (13)$$

The matrixes  $C_b^n(k-1)$ , and  $E_b^n(k-1)$  represent the cosine direction, and the rotation rate conversion from the body to the navigation frame.  $g^n$  is the gravity in the navigation frame.

The equations of the state vector correction using Mono-SLAM data are illustrated by the following equations: (14), (15) and (16).

$$K_{v,k}^{Kalman} = P_k^- H_v^T (H_v P_k^- H_v^T + R_v)^{-1} \quad (14)$$

$$Y_{v/i,k} = \hat{Y}_{v,k} + K_{v,k}^{Kalman} (\hat{Y}_{v,k} - Y_{vm,k}) \quad (15)$$

$$P_k = (I_{16} - K_{v,k}^{Kalman} H_v) P_k^- \quad (16)$$

The equations of state vector correction using IMU data are illustrated by the following equations (17), (18) and (19).

$$K_{i,k}^{Kalman} = P_k^- H_i^T (H_i P_k^- H_i^T + R_i)^{-1} \quad (17)$$

$$Y_{v/i,k} = \hat{Y}_{i,k} + K_{i,k}^{Kalman} (\hat{Y}_{i,k} - Y_{im,k}) \quad (18)$$

$$P_k = (I_{16} - K_{i,k}^{Kalman} H_i) P_k^- \quad (19)$$

Where  $K_{v,k}^{Kalman}$ , and  $K_{i,k}^{Kalman}$  are defined *Kalman* gains for *vision* and *IMU* measurements.

The two matrixes  $R_v$ , and  $R_i$  are the noise covariance associated with Mono-SLAM and IMU measurements. The covariance matrix update is defined by  $P_k$ .

### 3.3 Smooth Variable Structure Filter Approach

The SVSF is a closed loop filter (predictor-corrector) proposed by S. Habibi (Habibi, 2007), developed on the base of variable structure theory and sliding mode concepts, its structure based principally on a prior, and posterior errors between prediction and observation of the state vector elements.

The advantages of SVSF estimator compared to EKF are the robustness and stability. The linearization of the system is not needed, and the noise model is not necessary. The disadvantages of this estimator are the non optimality as all nonlinear filters, the chattering, and the choice of the superior limit of incertitude.

The previous prediction model (1) and (2) is utilized. The state vector elements are initialized by  $Y_{v/i,0}$  and the posterior error of estimation  $E_{0/0}$ . The update of our process is performed by using the two considered measurements which are given by (6) and (9). At a time, we use Mono-SLAM output, and at another time the IMU. In this case, another observation matrixes are used  $H_v = I_{16}$ , and  $H_i = I_{16}$ , these changes are due to the concept of SVSF mechanism.

The IMU vector measurements are given by the following equation (20).

$$Z_{IMU,k} = [X_{IMU} \quad V_{IMU} \quad a_{IMU} \quad \phi_{IMU} \quad \dot{\phi}_{IMU} \quad 0]^T \quad (20)$$

Where  $X_{IMU,k}$ ,  $V_{IMU,k}$ ,  $a_{IMU,k}$ ,  $\phi_{IMU,k}$ , and  $\dot{\phi}_{IMU,k}$  are the position, the velocity, the acceleration, the Euler angles, and the angular rate vectors defined in the

navigation frame. The acceleration and angular rate vectors are synthesized using the INS mechanization (12) and (13) based on temporal integration.

In the first process update, we use Mono-SLAM output based on the following equations (21), (22), (23), and (24).

$$E_{v,k/k-1} = \hat{Y}_{v,k} - Y_{vm,k/k-1} \quad (21)$$

$$K_{v,k}^{SVSF} = H_v^+ \text{diag} \left[ (|E_{v,k/k-1}|_{Abs} + \gamma |E_{k-1/k-1}|_{Abs})^\circ \right. \\ \left. \text{sat}(\bar{\Psi}^{-1} E_{v,k/k-1}) \right] \cdot [\text{diag}(E_{v,k/k-1})]^{-1} \quad (22)$$

The sign  $^\circ$  is the Schur operator (vector of element by element multiply). *Sat* is the saturation function. The notation *Abs* means absolute value.

$$Y_{v/i,k/k} = Y_{v,k} + K_{v,k}^{SVSF} E_{v,k/k-1} \quad (23)$$

$$E_{k/k} = \hat{Y}_{v,k} - Y_{v/i,k/k} \quad (24)$$

In the second, the IMU data are utilized to update the state vector elements based on the following equations (25), (26), (27), and (28).

$$E_{i,k/k-1} = \hat{Y}_{i,k} - Y_{im,k/k-1} \quad (25)$$

$$K_{i,k}^{SVSF} = H_i^+ \text{diag} \left[ (|E_{i,k/k-1}|_{Abs} + \gamma |E_{k-1/k-1}|_{Abs})^\circ \right. \\ \left. \text{sat}(\bar{\Psi}^{-1} E_{i,k/k-1}) \right] \cdot [\text{diag}(E_{i,k/k-1})]^{-1} \quad (26)$$

$$Y_{v/i,k/k} = Y_{i,k} + K_{i,k}^{SVSF} E_{i,k/k-1} \quad (27)$$

$$E_{k/k} = \hat{Y}_{i,k} - Y_{v/i,k/k} \quad (28)$$

Where  $(E_{v,k/k-1}, E_{i,k/k-1})$ ,  $E_{k/k}$  define prior and posterior errors,  $K_{v,k}^{SVSF}$ , and  $K_{i,k}^{SVSF}$  are the SVSF gains calculated in case of vision and IMU observation  $H_v^+$ , and  $H_i^+$  are the pseudo inverses of the two observation matrixes (Mono-SLAM and IMU) for the vision and inertial measurements, the parameter  $\gamma \in R^{16 \times 16}$  ( $0 < \gamma \leq 1$ ) is a diagonal matrix, its diagonal elements define the convergence rate of the state vector elements. In our work, it is supposed the following value  $\gamma = 0.5 \times I_{16}$ .

The diagonal matrix  $\bar{\Psi}^{-1}$  represents the inverse of  $\bar{\Psi}$ . This last is a boundary constructed with respect to the smoothing boundary layer vector.

$$\bar{\Psi}^{-1} = \begin{pmatrix} 1/\psi_{1,1} & \cdots & 0 \\ \vdots & \ddots & \vdots \\ 0 & \cdots & 1/\psi_{16,16} \end{pmatrix} \quad (29)$$

### 3.4 Combined SVSF-EKF Approach

The SVSF is a robust estimator compared to EKF. The author S. Habibi suggests to combine SVSF and EKF (Habibi, 2008) to improve estimator performance. The author, based on the variable structure filter (VSF) enforces the estimated elements to enter into the smooth boundary layer. Inside the boundary layer, the EKF is involved as a primary actor of estimation. We use the same model of prediction given by (1) and (2).

The two measurement vectors provided by Mono-SLAM and IMU boxes are similar to (6) and (9). The observation matrixes are those utilized in Sect. 3.3.

The combined SVSF-EKF gains are represented by the following equations (30) and (31).

$$k_{v,k}^C = \left( H_v^+ \left| (|E_{v,k/k-1}|_{Ab} + \gamma |E_{k-1/k-1}|_{Ab}) \right. + \Pi \right|_{Ab} \right) \\ \circ \text{sat}(K_{v,k}^{Kalman} \cdot E_{v,k/k-1}, 1) \quad (30)$$

$$k_{i,k}^C = \left( H_i^+ \left| (|E_{i,k/k-1}|_{Ab} + \gamma |E_{k-1/k-1}|_{Ab}) \right. + \Pi \right|_{Ab} \right) \\ \circ \text{sat}(K_{i,k}^{Kalman} \cdot E_{i,k/k-1}, 1) \quad (31)$$

The correction of the state vector elements are calculated by the following manner (32) and (33); where  $K_{v,k}^{Kalman}$ , and  $K_{i,k}^{Kalman}$  are the EKF gains with respect to vision and IMU measurements calculated by (14) and (17). The notation *Ab* means absolute value.

$$Y_{v/i,k/k} = Y_{v,k} + k_{v,k}^C E_{v,k/k-1} \quad (32)$$

$$Y_{v/i,k/k} = Y_{i,k} + k_{i,k}^C E_{i,k/k-1} \quad (33)$$

It is supposed  $\Pi = 0.9 \times I_{16}$  because, this matrix of factors defines the magnitude of EKF dominating inside the boundary layer. It must be higher than  $\gamma$  in order to emphasize *Kalman* action within the boundary layer.

### 3.5 Adaptive Smooth Variable Structure Filter Approach

An adaptive estimator version can provide better scale estimation in terms of robustness and accuracy. The ASVSF (Gadsden and Habibi, 2010; Gadsden et al., 2011)( adaptive smooth variable structure filter) utilizes the covariance matrix in order to have an idea about the probability of the estimated elements. The new version of SVSF is defined by the covariance matrix derivative and an optimal boundary layer matrix

$\bar{\Psi}^{opt}$ . The boundary layer matrix (29) being not diagonal, by including a full derivation of the covariance matrix (Hol et al., 2007). The boundary layer  $\bar{\Psi}^{opt}$  is obtained by: (34), which is given by: (35).

$$\frac{\partial(\text{trace}[P])}{\partial \bar{\Psi}} = 0 \quad (34)$$

$$\bar{\Psi}^{opt} = \begin{pmatrix} \Psi_{1,1} & \cdots & \Psi_{1,16} \\ \vdots & \ddots & \vdots \\ \Psi_{16,1} & \cdots & \Psi_{16,16} \end{pmatrix} \quad (35)$$

In case of ASVSF we follow the same steps defined by Subsection. 3.3. The difference is in the utilization of the covariance matrix to calculate the boundary layer as given by (36) and (37). The correction part of the ASVSF filter needs the linearization of the observation matrixes to calculate the optimal boundary layer (35).

$$\bar{\Psi}_{v,k}^{opt} = (H_v P_k H_v^T + R_v) (H_v P_k H_v^T)^{-1} \cdot \left[ \text{diag} \left( |E_{v,k/k-1}|_{Abs} + \gamma |E_{k-1/k-1}|_{Abs} \right) \right] \quad (36)$$

$$\bar{\Psi}_{i,k}^{opt} = (H_i P_k H_i^T + R_i) (H_i P_k H_i^T)^{-1} \cdot \left[ \text{diag} \left( |E_{i,k/k-1}|_{Abs} + \gamma |E_{k-1/k-1}|_{Abs} \right) \right] \quad (37)$$

$$K_{v,k}^{ASVSF} = H_v^+ \text{diag} \left[ \left( |E_{v,k/k-1}|_{Abs} + \gamma |E_{k-1/k-1}|_{Abs} \right)^\circ \cdot \text{sat} \left( \left( \bar{\Psi}_{v,k}^{opt} \right)^{-1} E_{v,k/k-1} \right) \right] \cdot \left[ \text{diag}(E_{v,k/k-1}) \right]^{-1} \quad (38)$$

$$K_{i,k}^{ASVSF} = H_i^+ \text{diag} \left[ \left( |E_{i,k/k-1}|_{Abs} + \gamma |E_{k-1/k-1}|_{Abs} \right)^\circ \cdot \text{sat} \left( \left( \bar{\Psi}_{i,k}^{opt} \right)^{-1} E_{i,k/k-1} \right) \right] \cdot \left[ \text{diag}(E_{i,k/k-1}) \right]^{-1} \quad (39)$$

The previous gains are used in (38) and (39) to provide the correction of state vector elements in (40) and (41).

$$Y_{v/i,k/k} = Y_{v,k} + K_{v,k}^{ASVSF} E_{v,k/k-1} \quad (40)$$

$$Y_{v/i,k/k} = Y_{i,k} + K_{i,k}^{ASVSF} E_{i,k/k-1} \quad (41)$$

The update of the covariance matrices in the case of vision and inertial measurement are given by: (42) and (43).

$$P_k = (I_{16} - K_{v,k}^{ASVSF} H_v) P^- (I_{16} - K_{v,k}^{ASVSF} H_v)^T + K_{v,k}^{ASVSF} R_v K_{v,k}^{ASVSF} \quad (42)$$

$$P_k = (I_{16} - K_{i,k}^{ASVSF} H_i) P^- (I_{16} - K_{i,k}^{ASVSF} H_i)^T + K_{i,k}^{ASVSF} R_i K_{i,k}^{ASVSF} \quad (43)$$

## 4 SIMULATION RESULTS

### 4.1 Evaluation Scenarios

We suggest four scenarios of scale variation. At first, an arbitrary trajectory (on Matlab software) was simulated of the couple (Camera/IMU), and it is taken into consideration the standard deviation noises supposed in Sect. 3.1. In the first scenario, the scale of the Mono-SLAM is considered as the absolute scale  $\lambda = 1$ , but we suggest a bad initialization  $\lambda_0 = 0.5$  (the scale initialization is an important point of scale estimation). The output graph is given by Fig. 2. We remark that the absolute scale estimation (by the four estimators) is recovered after 8 seconds despite starting with a worst case. ALL approaches stabilize in the absolute scale after 8 seconds with an average error of 0.8% due to the noises affecting the other state vector elements. In terms of approaches comparison, the different estimators retrieve the absolute scale by almost the same performance despite the bad initialization. In the second scenario, it is supposed the same steps of the previous scenario, but after scale value stabilization  $\lambda \approx 1 \pm 0.8\%$ , an atypical value was included ( $\lambda = 0.8$ ) of scale to compare the robustness of the four estimators against outliers. In Fig. 3, we notice that Combined SVSF-EKF approach is more robust than EKF, SVSF, and ASVSF in front of briskly atypical scale value. In case of scale estimation, the ASVSF solution does not provide a good result compared to Combined SVSF-EKF. This result is due to the scale noise nature at a time, and the concept of variable structure combined with Kalman filter in another time. For a deep comparison, the ASVSF found the scale with a performance near Combined SVSF-EKF estimator, and also it gives the scale incertitude for each scale value estimated. In the third scenario, we suppose just that the Mono-SLAM output is affected by a scale factor  $\lambda = 1 + n$  with  $n$  is a noise of standard deviation  $\sigma_n = 10^{-4}$ . The aim of this scenario is to show the behavior and stability of the proposed approaches in front of a scale with a noise. The result is given by Fig. 4, we see that all estimators resist against scale fluctuation, and show a considerable stability in case of scale with fulfillment to the small standard deviation value of scale noise. To go further, a comparison is performed later which will provide a deep analysis about stability and robustness. It is considered in the fourth scenario, that the output of the Mono-SLAM box is equal to the absolute scale plus a sinusoidal variation  $\lambda = 1 + (1/40) \cdot \sin \theta$ , with  $\theta$  is an angle of value 0 to 360 degrees. The purpose of this scenario is to show the capability of scale tracking by the four estimators. The result is given by Fig.

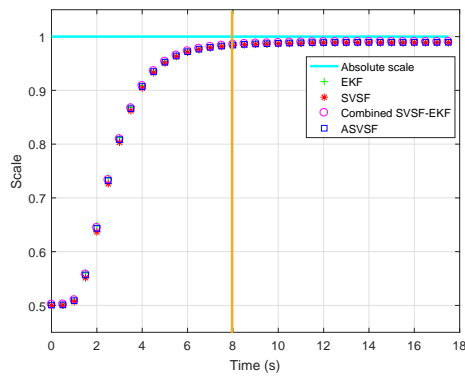


Figure 2: The first scenario of scale estimation using EKF, SVSF, Combined SVSF-EKF, and ASVSF.

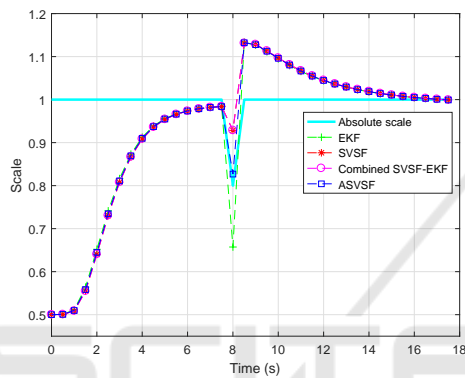


Figure 3: The second scenario of scale estimation using EKF, SVSF, Combined SVSF-EKF, and ASVSF.

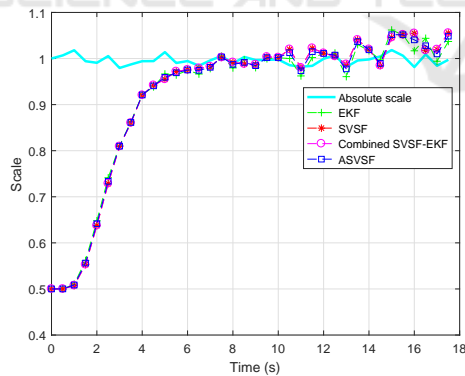


Figure 4: The third scenario of scale estimation using EKF, SVSF, Combined SVSF-EKF, and ASVSF.

5. It is remarkable that the Combined SVSF-EKF is more accurate than the other estimators in terms of scale tracking. By comparison of all proposed estimators, we remark that, we have not a big difference in terms of tracking, but this difference can be significantly larger in case of the long trajectory.

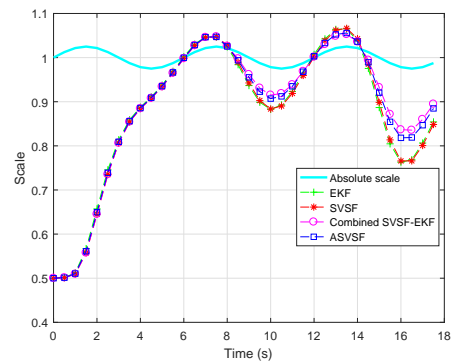


Figure 5: The fourth scenario of scale estimation using EKF, SVSF, Combined SVSF-EKF, and ASVSF.

## 4.2 Performances Analysis

We try to give an indepth analysis of the proposed estimators for scale estimation in terms of robustness, stability, and accuracy based on the appropriate measurement tools.

### 4.2.1 Robustness and Stability Analysis

To assess the robustness and stability measurement (Maronna et al., 2006) of each estimator, the following manner is adopted; the Mono-SLAM scale is supposed to be affected by noise of standard deviation  $\sigma_n = 10^{-4}$ . A point is selected in the middle of scale estimation process (this point has a typical scale around the absolute scale), this last was changed by an atypical scale. The value of this outlier is augmented gradually until 100 percent of the scale contamination. The experience is repeated many times to get significant results. At the end, we measure the maximum bias of scale deviation compared to the absolute scale for the four estimators using the formula (44).

$$\lambda_b^{Max} = \max |\lambda_i - \lambda_{Ref}| \quad (44)$$

Where  $\lambda_{Ref}$  is the scale reference without contamination, and  $\lambda_b^{Max}$  signifies the bias max of scale deviation of a given contamination, the term  $\lambda_i$  is the scale value in the case of the same contamination measured many times ( $i$  times). The results are given by the graph in Fig. 6. It is remarkable that, all the estimators involved in scale recovering lost their robustness significantly according to scale contamination until instability of scale recovery process. The best estimator in terms of robustness is the Combined SVSF-EKF due to the synergy provided by the couple SVSF-EKF. After, comes the ASVSF because it has the variable structure force with an optimal gain ensured by the variable boundary layer. The SVSF presents also a significant robustness under the ASVSF but better than the classical solution (EKF). The maximum scale

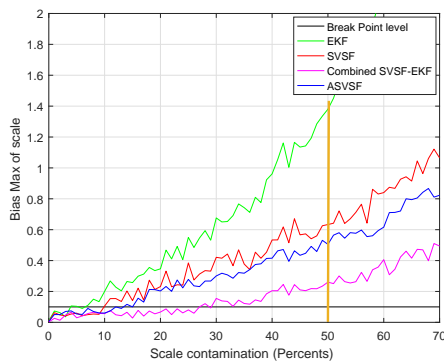


Figure 6: The robustness and stability analysis of EKF, SVSF, Combined SVSF-EKF, and ASVSF.

bias deviation allowed by scale recovery process depends on the application. However, in our work, we suggest that the bias max of scale tolerance is equal to 0.1. It is remarkable that the Combined SVSF-EKF has the best break point which is around 30%, the ASVSF is about 15%, the SVSF is approximately 10%, and EKF is under 10%. Beyond these scale contaminations' values, the robustness of the proposed estimators are not guaranteed with respect to the maximum scale deviation supposed. In case of scale contamination of 50 percent, the maximum deviation of scale bias deviation does not exceed 0.3 for the Combined SVSF-EKF approach. In case of ASVSF, the deviation is approximately 0.5, for SVSF is about 0.6, and in the classical method the maximal deviation of scale bias is 1.4 (this means instability of the scale method). For the robust filter (SVSF, Combined SVSF-EKF, and ASVSF) the stability of our system is guaranteed compared to the EKF approach. But, it is recommended to select the ASVSF estimator, because it brings together many advantages as the robustness, the accuracy, the uncertainty information, and the respect of the real time constraint.

#### 4.2.2 Accuracy Analysis

To analyze the accuracy and to give a quantification of the precision range of our methods, we try to measure the accuracy of the suggested estimators by considering the following steps. The scale is affected by noise of a standard deviation  $\sigma_n = 10^{-4}$ . Some points of the scale estimation system are replaced by outliers near scale tolerance (these scale values can be supported easily by our proposed system) of value equal to 0.12 (in these points the scale becomes  $\lambda = 0.88$ ). The number of points touched by scale outliers is increased gradually to 100 percent. For each contamination, we calculate the corresponding average of the root-mean-square error (RMSE). The graph of accuracy measurement is given by Fig. 7. It is remarkable

Table 1: The means RMSE of EKF, SVSF, Combined SVSF-EKF, and ASVSF.

Est	EKF	SVSF	Combined	ASVSF
Mean	0.084	0.086	0.085	0.086

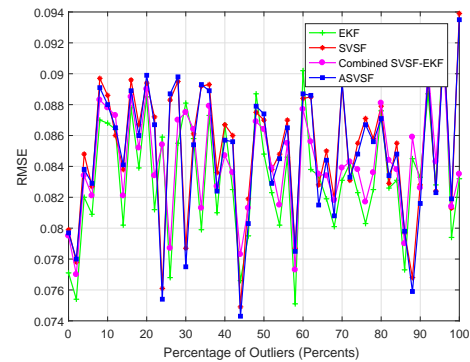


Figure 7: The accuracy analysis of EKF, SVSF, Combined SVSF-EKF, and ASVSF.

that the Combined SVSF-EKF is near optimal performance of the famous estimator EKF. There is not a big difference between SVSF and ASVSF in terms of accuracy, so it depends on the application in which it is involved (in case of searching for high precision). The graph of RMSE in case of ASVSF is near to the Combined SVSF-EKF, so it is preferable to select the ASVSF instead of the Combined SVSF-EKF despite the superiority presented because, at least the ASVSF provides an idea about the uncertainty of the scale value. To understand better the Fig. 7, the Table 1 is proposed which gives a summary of the means RMSE for the four estimators proposed. The RMSE of all the estimators is numerically close, but in case of the scale value, the least difference is considerable.

## 5 EXPERIMENT RESULTS

### 5.1 The Environment of Experiment

The experiment results are realized by using a dataset of a micro aerial vehicle (MAV) (an AscTec Firefly hex-rotor helicopter). This MAV has two monochrome front-down looking Cameras type MT9V034 of a rate 20 Hz and an IMU type ADIS16448 of MEMS technology with a rate of 200 Hz. The standard deviations of noises, biases, and the frequencies of IMU are given in the Methodology section. For more details about the system configuration, refer to (Burri et al., 2016).

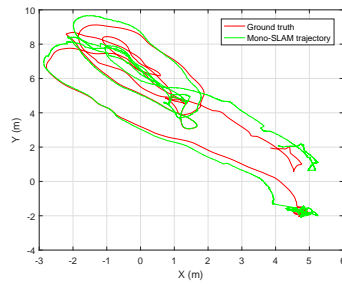


Figure 8: The top view of the trajectory obtained by the Mono-SLAM and the ground truth in case of a real data (MH 01 easy).

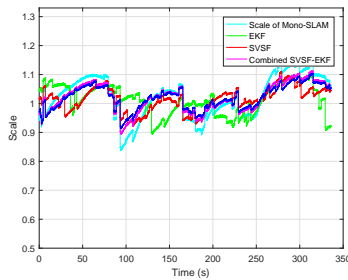


Figure 9: The scale estimation using EKF, SVSF, Combined SVSF-EKF and ASVSF in case of a real data (MH 01 easy).

## 5.2 The Scale Recovering of a Real Data

To obtain the up to scale trajectory, we applied on the image of the dataset a well known Mono-SLAM named inverse depth parameterization for monocular SLAM (Civera et al., 2008). This Mono-SLAM is based essentially on the EKF. The brute force of this solution is the representation of the depth by its inverse form. However, it allows to handle uncertainty accurately during undelaying initialization and beyond. As all kinds of Mono-SLAM, it provides a trajectory with an unknown scale as given by Fig. 8. We applied the fourth proposed estimators to recover the absolute scale on this up to scale trajectory as given by Fig. 9. This figure shows the superiority of scale recovering of the robust filter against the classical solution (EKF). The Fig. 10 shows the 3D trajectory of the MAV (ground truth) and the estimated trajectories realized by the four estimators (EKF, SVSF, Combined SVSF-EKF and ASVSF) in case of a real data (MH 01 easy). To provide a clear comparison between all the estimators, we suggest to calculate the RMSE for all these estimators as given by Fig. 11. The robust filter provides a good result in term of scale tracking in case of real data. This judgment stays valid for the other scenarios choices from the dataset (MH 01 easy, MH 03 medium, and MH 05 difficult) as given by the Table 2. The RMSE for the four estimators degraded systematically by the quality of frames acquired from the explored environment, this limitation is due to the

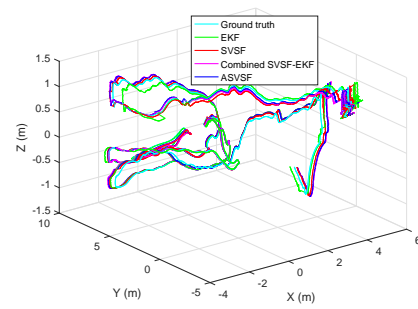


Figure 10: The 3D trajectories of ground truth, EKF, SVSF, Combined SVSF-EKF and ASVSF in case of a real data (MH 01 easy).

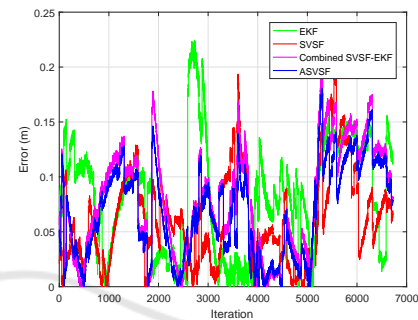


Figure 11: The RMSE of trajectories for EKF, SVSF, Combined SVSF-EKF and ASVSF in case of a real data (MH 01 easy).

Table 2: The mean RMSE of scale estimation using EKF, SVSF, Combined SVSF-EKF, and ASVSF in case of a real data (MH 01 easy, MH 03 medium, and MH 05 difficult)

	MH 01	MH 03	MH 05
Length (m)	80.6	130.9	97.6
Duration (s)	182	132	111
Mean EKF	0.0857	0.0987	0.0997
Mean SVSF	0.0590	0.0773	0.0882
Mean Combined	0.0319	0.0468	0.0643
Mean ASVSF	0.0425	0.0564	0.0725

high perturbation of scale which is affected by the low textured or darkness of frames acquired.

## 5.3 The Real Time Evaluation

The environment of development is Matlab, installed into a computer of a characteristic; Intel(R) Core (TM), processor i5 of frequency 2.40 GHz. In our work, the scale is recovered into a multi-rate mechanism. However, the Mono-SLAM utilized in our work provides an up to scale trajectory in real time of frequency 20 Hz. Our solutions permit to estimate the

Table 3: The frequency of scale estimation for EKF, SVSF, Combined SVSF-EKF, and ASVSF

Est	EKF	SVSF	Combined	ASVSF
Freq	93 Hz	105 Hz	88 Hz	97 Hz

scale many times between two poses, this mean that it is possible to do another estimation stage in a period of about 50 ms. From the Table 3, we note that the scale value is improved within a frequency bigger than the vision part. But, this frequency, depends essentially on the mathematical formulation for each estimator. The frequency of estimation can not be evaluated separately from the scale estimation quality. Sure, that SVSF is the better in terms of frequency, but, it is not the best in term of RMSE. The Combined SVSF-EKF is a good estimator but also it is not the fastest. The ASVSF can be considered as a good estimator of scale because it allows to recover the scale in real time with a rate of about 97 Hz and a scale near Combined SVSF-EKF quality.

## 6 CONCLUSIONS

This paper focused on a timely problem which relies to the Mono-SLAM field. It treats the scale recovering into a multi-rate fusion scheme. We have implemented, and compared four approaches of scale estimation: EKF, SVSF, Combined SVSF-EKF, and ASVSF. The obtained results of this work, showed a significant performance of robust filters (SVSF, Combined SVSF-EKF, and ASVSF) against the classical solution (EKF) in terms of scale factor recovering and real time constraint. The different results obtained permit to focus on the Combined SVSF-EKF method which provides a compromise between robustness and accuracy. But, in terms of real time constraint, it is better to utilize the ASVSF estimator. In addition, the ASVSF is near performance of the Combined SVSF-EKF, and also it provides an assesses about the incertitude of scale estimation as in the case of the EKF. In this work, we showed that the filtering process into multi-rate mechanism allows the determination of the scale factor with a rate superior than the vision system 20 Hz especially for SVSF, and ASVSF. As a future work, we plan to design from scratch a new Mono-SLAM system with some new ideas and to involve our solution to estimate the scale. The complete system can be embedded easily onto a MAV in order to navigate safely. In the same subject studied in this paper, we propose to design another system by many sensors and studying the fault tolerance of the developed system.

## REFERENCES

- Agrawal, M. and Konolige, K. (2006). Real-time localization in outdoor environments using stereo vision and inexpensive *GPS*. In *International Conference on Pattern Recognition*, pages 1063–1068.
- Armesto, L., Chroust, S., Vincze, M., and Tornero, J. (2004). Multi-rate fusion with vision and inertial sensors. In *Robotics and Automation, Proceedings. ICRA'04 International Conference on*, volume 1, pages 193–199. IEEE.
- Botterill, T., Mills, S., and Green, R. (2013). Correcting scale drift by object recognition in single-camera *SLAM*. *IEEE transactions on cybernetics*, 43(6):1767–1780.
- Burri, M., Nikolic, J., Gohl, P., and Schneider, T. (2016). The euroc micro aerial vehicle datasets. *The International Journal of Robotics Research*, 35(10):1157–1163.
- Civera, J., Davison, A., and Montiel, J. (2008). Inverse depth parametrization for monocular *SLAM*. *IEEE transactions on robotics*, 24(5):932–945.
- Davison, A., Reid, I., and Molton, N. (2007). Mono *SLAM*: Real-time single camera *SLAM*. *IEEE Transactions on Pattern Analysis & Machine Intelligence*, (6):1052–1067.
- Dumortier, Y., Benenson, R., and Kais, M. (2006). Real-time vehicle motion estimation using texture learning and monocular vision. In *International Conference on Computer Vision and Graphics ICCVG*.
- Eade, E. and Drummond, T. (2006). Scalable monocular *SLAM*. In *Computer Vision and Pattern Recognition, 2006 IEEE Computer Society Conference on*, volume 1, pages 469–476. IEEE.
- Engel, J. and Cremers, D. (2014). Lsd-*SLAM*: Large-scale direct monocular *SLAM*. In *European Conference on Computer Vision*, pages 834–849. Springer.
- Forste, C., Lynen, S., Kneip, L., and Scaramuzza, D. (2013). Collaborative monocular *SLAM* with multiple micro aerial vehicles. In *International Conference on Intelligent Robots and Systems on*, pages 3962–3970. IEEE.
- Frost, D., Kahler, O., and Murray, D. (2016). Object-aware bundle adjustment for correcting monocular scale drift. In *Robotics and Automation (ICRA), International Conference on*, pages 4770–4776. IEEE.
- Gadsden, S. and Habibi, S. (2010). A new form of the smooth variable structure filter with a covariance derivation. In *Decision and Control (CDC), 49th Conference on*, pages 7389–7394. IEEE.
- Gadsden, S., Sayed, M. E., and Habibi, S. (2011). Derivation of an optimal boundary layer width for the smooth variable structure filter. In *American Control Conference (ACC)*, pages 4922–4927. IEEE.
- Grater, J., Schwarze, T., and Lauer, M. (2015). Robust scale estimation for monocular visual odometry using structure from motion and vanishing points. In *Intelligent Vehicles Symposium (IV), 2015 IEEE*, pages 475–480. IEEE.

- Gutierrez-Gomez, D., Puig, L., and Guerrero, J. (2012). Full scaled 3d visual odometry from a single wearable omnidirectional camera. In *Intelligent Robots and Systems (IROS), RSJ International Conference on*, pages 4276–4281. IEEE.
- Habibi, S. (2007). The smooth variable structure filter. *Proceedings of the IEEE*, 95(5):1026–1059.
- Habibi, S. (2008). Combined variable structure and Kalman filtering approach. In *American Control Conference, 2008*, pages 1855–1862. IEEE.
- Hol, J., Schon, T., Luinge, H., and Gustafsson, F. (2007). Robust real-time tracking by fusing measurements from inertial and vision sensors. *Journal of Real Time Image Processing*, 02(02):149–160.
- Ikedada, S., Sato, T., and Yamaguchi, K. (2007). Construction of feature landmark database using omnidirectional videos and GPS positions. In *International Conference on Pattern Recognition*, pages 249–256. IEEE.
- Jung, S. and Taylor, C. (2001). Camera trajectory estimation using inertial sensor measurements and structure from motion results. In *Proceedings of the IEEE Computer Society Conference on Computer Vision and Pattern Recognition*, pages 732–737.
- Kitt, B., Rehder, J., Chambers, A., and Schonbein, M. (2007). Monocular visual odometry using a planar road model to solve scale ambiguity. In *Proc of European Conference on Mobile Robots*.
- Klein, G. and Murray, D. (2007). Parallel tracking and mapping for small ar workspaces. In *Mixed and Augmented Reality, ISMAR, 6th IEEE and ACM International Symposium on*, pages 225–234. IEEE.
- Kobzili, E., Larbes, C., and Allam, A. (2017a). Multi-rate robust scale estimation of monocular SLAM. In *Systems and Control (ICSC), 6th International Conference on*, pages 1–5. IEEE.
- Kobzili, E., Larbes, C., and Allam, A. (2017b). Robust absolute scale estimation of monocular SLAM using a combined svsf-ekf strategy for mav navigation. In *1st Algerian Multi-Conference on Computer, Electrical and Electronic Engineering*. USTHB of Algiers.
- Lemaire, T., Berger, C., Jung, I., and Lacroix, S. (2007). Vision-based SLAM: Stereo and monocular approaches. *International Journal of Computer Vision*, 74(3):343–364.
- Lothe, P. (2010). *Simultaneous localization and mapping with monocular vision constraint with SIG*. PhD thesis, University of Blaise Pascal Clermont-Ferrand II, France.
- Maronna, R., Martin, R., and Yohai, V. (2006). Robust statistics. Wiley Chichester.
- Montemerlo, M. (2003). A factored solution to the simultaneous localization and mapping problem with unknown data association. *Ph. D. thesis, Carnegie Mellon University, Pittsburgh*.
- Mur-Artal, R., Montiel, J., and Tardos, J. (2015). Orb-SLAM: a versatile and accurate monocular SLAM system. *IEEE Transactions on Robotics*, 31(5):1147–1163.
- Nemra, A. (2011). Robust airborne 3d visual simultaneous localisation and mapping. *Ph. D. thesis, Cranfield University, England*.
- Nister, D., Naroditsky, O., and Bergen, J. (2006). Visual odometry for ground vehicle applications. *Journal of Field Robotics*, 23(1):3–20.
- Nutzi, G., Weiss, S., Scaramuzza, D., and Siegwart, R. (2011). Fusion of imu and vision for absolute scale estimation in monocular SLAM. *Journal of intelligent & robotic systems*, 61(1-4):287–299.
- Pillai, S. and Leonard, J. (2015). Monocular SLAM supported object recognition. In *Computer Vision and Pattern Recognition*.
- Pirker, K., R  ther, M., and Bischof, H. (2011). Cd SLAM-continuous localization and mapping in a dynamic world. In *Intelligent Robots and Systems (IROS), 2011 IEEE/RSJ International Conference on*, pages 3990–3997. IEEE.
- Qiang, L., Jianye, M., Guosheng, W., and Huican, L. (2016). Absolute scale estimation of orb-SLAM algorithm based on laser ranging. In *Robotics and Automation (ICRA), International Conference on*, pages 10279–10283. IEEE.
- Scaramuzza, D., Fraundorfer, F., Pollefeys, M., and Siegwart, R. (2009). Absolute scale in structure from motion from a single vehicle mounted camera by exploiting nonholonomic constraints. In *Computer Vision, 12th International Conference on*, pages 1413–1419. IEEE.
- Scaramuzza, D. and Siegwart, R. (2008). Appearance-guided monocular omnidirectional visual odometry for outdoor ground vehicles. *IEEE transactions on robotics*, 24(5):1015–1026.
- Simond, N. and Rives, P. (2004). Trajectory of an uncalibrated stereo rig in urban environments. *Intelligent Robots and Systems, 2004.(IROS 2004). Proceedings. 2004 IEEE/RSJ International Conference on*, (4):3381–3386.
- Smith, R., Self, M., and Cheeseman, P. (1990). Estimating uncertain spatial relationships in robotics. In *Autonomous robot vehicles*, pages 167–193. Springer.
- Song, S. and Chandraker, M. (2014). Robust scale estimation in real-time monocular sfm for autonomous driving. In *Proceedings of the IEEE Conference on Computer Vision and Pattern Recognition*, pages 1566–1573.
- StreLOW, D. and Singh, S. (2004). Motion estimation from image and inertial measurements. *International Journal of Robotique Research*, 23(12):1157–1195.
- Weiss, S. and Siegwart, R. (2011). Real-time metric state estimation for modular vision-inertial systems. In *International Conference on Robotics and Automation:(ICRA 2011)*, pages 4531–4537. IEEE.
- Zachariah, D. and Jansson, M. (2011). Self-motion and wind velocity estimation for small-scale uavs. In *Robotics and Automation (ICRA), International Conference on*, pages 1166–1171. IEEE.